PCCP

RSC Publishing

PAPER

View Article Online
View Journal | View Issue

Cite this: *Phys. Chem. Chem. Phys.*, 2013, **15**, 10761

Enhanced field emission characteristics in metal-coated Si-nanocones

Yuan-Ming Chang,*[a] Pin-Hsu Kao,[b] Hung-Ming Tai,[b] Hau-Wei Wang,[b] Chih-Ming Lin,[c] Hsin-Yi Lee[de] and Jenh-Yih Juang*[a]

Received 3rd March 2013,
Accepted 25th April 2013

DOI: 10.1039/c3cp50948f

www.rsc.org/pccp

Metallic gold (Au) and platinum (Pt) thin films were deposited on silicon nanocones (Si-NCs) by sputtering to elucidate the effects of work function and conductivities on the field electron emission characteristics of surface-modified Si-NCs. The results showed that for Pt/Si-NCs and Au/Si-NCs, although the turn-on field defined at a corresponding current density of 10 μA cm^{-2} only improved from 4.20 V μm^{-1} for bare Si-NCs to 3.65 and 2.90 V μm^{-1}, respectively, the emission current density measured at 5.00 V μm^{-1} was enhanced by orders of magnitude, reaching 1.82 mA cm^{-2} for Au/Si-NCs. Compared to those obtained from various surface-modified Si-nanostructures, such as ZnO/Si-nanopillars and ferroelectrics/Si-nanotips, the current results represent an interesting alternative route for producing surface-modified Si-NCs that might be useful for optical and electronic applications.

Introduction

The remarkable optical and electronic properties obtained in various one-dimensional (1D) Si-nanostructures (Si-NSs), including nanowires,[1] nanotubes,[2] and nanorods,[3,4] have made the 1D Si-NSs one of the most hotly pursued candidates for high-performance electronic devices.[5] Of particular interest is the anticipated enhancement in electron field emission from 1D Si-NSs and the compatibility with the mature Si-based technologies, which might bring a variety of modern applications into reality, such as active field emitters for high current X-ray sources and field emission displays.[6] Consequently, considerable efforts have been devoted to fabricate Si-based field-emitters with low turn-on fields and high emission current densities. Unfortunately, most of the as-prepared 1D Si-NSs have been falling short in meeting these requirements, presumably due to the inevitable influences from the native silicon oxides formed on the surface of various Si-NSs. In order to improve the field emission properties of Si-NSs, various approaches were developed.[7–17] For instance, various ferroelectric oxides[18,19] have been coated on the pre-fabricated Si-NSs in trying to take the advantage of low electron affinity and polarization induced electric fields at the interface, both are conceived to be beneficial to electron emissions. Alternatively, semiconductor thin films grown by atomic layer deposition (ALD)[20] were coated onto the Si-NSs to improve their field emission characteristics. Drastic improvements in both the turn-on voltage and emission current densities had been indeed obtained in ALD-derived ZnO/Si-nanopillar structures.[20] The abovementioned approaches, however, are either involving complex manufacturing processes or requiring high fabrication temperatures (>200 °C), thus might be difficult to be fully integrated with the contemporary Si-technologies. It is thus desirable to develop an efficient method for obtaining 1D Si-related nanostructure with much improved functionalities.

The present study reports a novel method of fabricating metal-coated Si-nanocone (Si-NC) arrays and the field emission characteristics obtained from these structures. The Si-NCs were generated by direct dry etching at a temperature of 60 °C, using the self-assembled silver (Ag) nanoislands as the metal masks. Since the self-assembled Ag nanoislands were obtained within 10 seconds by single-step sputtering at ambient temperature and no lithography was needed in the subsequent dry etching process, the current method is thus far more efficient and cost-effective than most of the previous processing methods adopted to fabricate Si-NSs. Moreover, the density of the 1D Si-NCs can be manipulated by adjusting the sputtering conditions for obtaining the Ag-nanoislands. This may turn out to be crucial in reducing the screening effects commonly encountered by many other 1D

[a] *Department of Electrophysics, National Chiao Tung University, Hsinchu 300, Taiwan. E-mail: ymchang7@gmail.com, jyjuang@g2.nctu.edu.tw*
[b] *Center for Measurement Standards, Industrial Technology Research Institute, Hsinchu 300, Taiwan*
[c] *Department of Applied Science, National Hsinchu University of Education, Hsinchu 300, Taiwan*
[d] *National Synchrotron Radiation Research Center, Hsinchu 300, Taiwan*
[e] *Department of Materials Science and Engineering, National Chiao Tung University, Hsinchu 300, Taiwan*

nanostructures, such as the bundled carbon nanotubes or catalytically grown ZnO nano-structures. Furthermore, it is known that the electric conductivity of the emitter may also play an important role in field emission properties. Thus, in order to enhance the field emission property of the obtained Si-NCs, gold (Au) and platinum (Pt) with thickness of 10–20 nm were, respectively, deposited on Si-NCs by sputtering to form metal/Si-NC heterostructures. The results indicate that metal coating can drastically enhance the emission current, albeit it appeared to only have a moderate effect in reducing the turn-on field of similar Si-NCs.

Experimental section

The Ag nanoislands grown on Si-substrates were obtained by rf-sputtering from an Ag target for 10 seconds with an input power of 150 W in a 25 sccm argon gas atmosphere. Due to the short sputtering time practiced, the resulting size distribution of the obtained Ag nanoislands is rather uneven. The Si-NC array was obtained by subsequent dry etching performed in a metal etcher system. Prior to etching, the chamber was evacuated to a base pressure of 3×10^{-5} Torr while the system temperature was kept at 60 °C. After loading the prepared Ag nanoisland covered Si-substrate, Cl_2 gas of 150 sccm and N_2 gas of 10 sccm were introduced. The system was operated at a fixed input power of 3000 W and the etching time lasted for 5 minutes. The Si-NCs were formed through the anisotropic etching resulting from persistent bombardments of the reactive ions accelerated toward the Si substrate. The Si substrate with Si-NCs was etched using a standard buffered oxide etch (BOE) for 5 minutes to ensure complete removal of the native oxides prior to carrying out the Au or Pt film deposition. For investigating the effects of metal coating, the Au and Pt thin films were deposited onto Si-NCs by rf-sputtering. Tapping-mode atomic force microscopy (AFM, Dimension 9000) and field-emission scanning electron microscopy (FESEM, JEOL JSM-6700F) were used to image the surface morphology of samples at various stages of fabricating Si-NC arrays. The detailed microstructures of the metal-coated Si-NCs were investigated using a cross-sectional transmission electron microscope (XTEM, JEOL JEM-2010F) with an operating voltage of 200 kV. To prepare the XTEM samples, the specimens were firstly cut from the stacked wafers of Au/Si-NCs, and then mechanically polished down to 20–30 μm-thick, followed by Ar ion milling to finally obtain electron transparency. Moreover, the samples were loaded into a vacuum chamber to measure the field-emission current. The phosphor (P_{22}), which was applied in the cathode-ray tube displays, was deposited on a transparent conductive material (indium-tin-oxide), to serve as the anode electrode in the vacuum system and the cathode voltage was applied to the Si substrates. The distance between the sample and the electrode is 200 μm and the chamber pressure being kept at 2×10^{-6} Torr during all the field-emission measurements.

Results and discussion

Fig. 1a shows the typical morphology and distribution of the Ag nanoislands obtained with a sputtering time of 10 seconds.

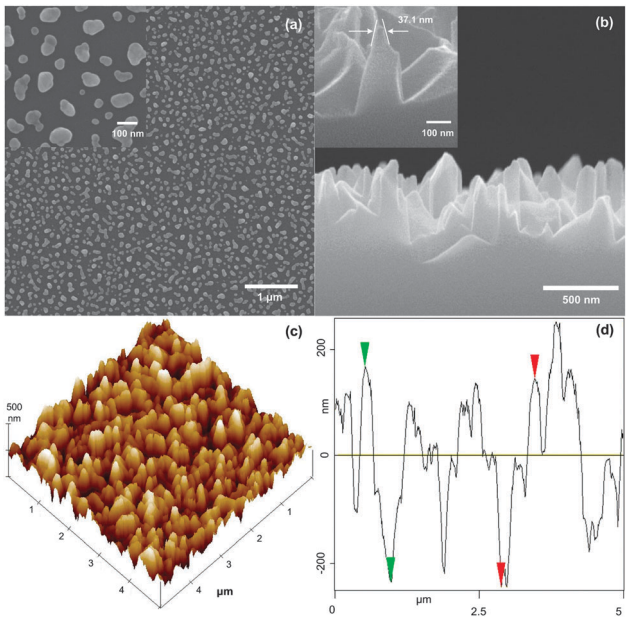

Fig. 1 The SEM images of (a) Ag nanoislands distributed on the Si-substrate. A higher magnification SEM image (the inset) shows the size distribution of the Ag nanoislands; (b) Si-NC array. The inset is a higher magnification SEM image of Au/Si-NCs, showing that the morphology of the Si-NC array is not changed by Au coating. (c) The three-dimensional AFM image of Au/Si-NCs; and (d) the profile of (c).

The density of the Ag nanoislands is estimated to be around 4.5×10^9 cm^{-2}. This characteristic is believed to arise from the film growth mechanism inherent to the current system and can be understood as follows. Since the surface energies for Ag and SiO_2 are about 923 ergs cm^{-2} and 200–260 ergs cm^{-2}, respectively,[21,22] one expects that the deposited Ag layer would follow the Volmer–Weber growth mode and grow into island-like morphology during the processes of sputtering. The nucleation and growth of the individual islands, thus, prevailed predominantly by surface diffusion of the impingement of condensate monomers, rather than the thermal-induced dewetting and subsequent agglomeration of an existing thin layer frequently observed in processes involving post-deposition annealing. Fig. 1b displays the well-aligned Si-NCs obtained from Si-substrates partially covered with the Ag nanoislands as shown in Fig. 1a after performing the dry etching process for 5 min. The Si-NCs obtained under this condition have an average height of 350–450 nm. Obviously, the Ag nanoislands acted as effective metal-nanomasks during the early stage of dry etching performed on the Si-substrate. The formation of Si-NCs thus was a natural consequence of the uneven protection from Ag nanoislands of various sizes, which provide different degrees of protection to the areas underneath from ion bombardment and led to significant anisotropic etching prevailing on the exposed areas of the Si-substrate. The inset of Fig. 1b shows a higher magnification SEM image of Au/Si-NCs. It is evident that Au-coating does not have any observable effect in changing the morphology of the Si-NC array. The surface morphology and the profile of the Au/Si-NC array were independently examined using AFM, as shown in Fig. 1c and d. These results are in good agreement with the SEM image shown in Fig. 1b.

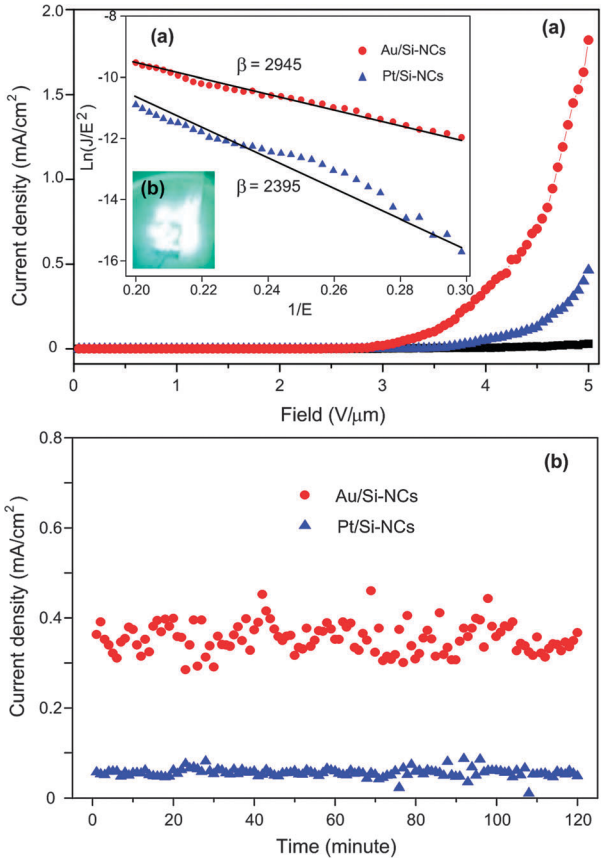

Fig. 2 (a) Field emission *J–E* curve from the Au (solid circles), Pt (solid triangles) on Si-NCs and the bare Si-NC array (black squares) at a working distance of 200 μm over an effective emitting area of 1 cm^2. The F–N plots [$\ln(J/E^2)$ *vs.* $(1/E)$] of Au/Si-NCs and Pt/Si-NCs are shown in the inset (a); the inset (b) shows a bright luminescence of Au/Si-NCs from a phosphor. (b) The emission current as a function of time operated at 4 V μm^{-1}, showing the robustness of the Au/Si-NC (solid circles) and Pt/Si-NC (solid triangles) nanostructures.

Fig. 2a shows the emission current density as a function of the applied electric field (*J–E* curves) for the bare Si-NCs (black squares), Pt/Si-NCs (blue triangles), and Au/Si-NCs (red circles), respectively. Here, the electric field was determined by dividing the applied voltage with the apparent cathode–anode separation of 200 μm. Thus, it is a measure of the average global field instead of the local field at the tips of the nanostructures. It is evident from Fig. 2a that, for the bare Si-NCs, only diminishingly small field emission current could be detected upto the maximum applied field (5 V μm^{-1}) available in our setup. This is presumably due to the existence of the native oxide layer existing at the surface of the as-prepared Si-NCs, which might form an insurmountable barrier for electron emission. We shall come back to this point later. On the other hand, as can be seen from the *J–E* plots in Fig. 2a, the turn-on fields, defined using the 10 μA cm^{-2} criterion, are reduced to 3.65 and 2.90 V μm^{-1} for Pt/Si-NCs and Au/Si-NCs, respectively.

Moreover, the emitted current density at a bias field of 5 V μm^{-1} is also dramatically enhanced from 0.02 mA cm^{-2} for the as-prepared Si-NCs to 0.47 mA cm^{-2} and 1.82 mA cm^{-2} for Pt/Si-NCs and Au/Si-NCs, respectively. Fig. 2b shows the emission current density as a function of time operated at 4 V μm^{-1} for Au/Si-NCs and Pt/Si-NCs. It is evident from the results that, although it appears to be fluctuating (presumably due to the simple circuitry of our measuring setup), the current density does not show any sign of diminishing over the 2 hours period of continuous testing. Together with the low turn-on field and high current density described above, the current Au/Si-NC core–shells can be regarded as excellent field emitters and should be of great potential for various field emission-associated applications. Compared to the field emission characteristics collected from the literature reported for varieties of Si-related nanostructures (Table 1),[6,18–20,23] it is evident that the Pt/Si-NC and Au/Si-NC structures presented in this study outperform most of them by a large margin, except for the very low turn-on field observed in ZnO/Si-NPs.[20] However, it is noted here that in the ZnO/Si-NPs[20] the average tip radius of the Si-NPs was only about 15 nm compared to ~30 nm in the present case. In any case, it is interesting to note that the enhancements acquired here are obtained by merely coating a thin metallic film to essentially the same Si-NCs. Considering the two primary factors dominating the field emissions of a particular emitter, namely the geometric factor and the effective work function, it should be interesting to further delineate the relevant factors giving rise to the current results.

Fig. 3 shows the XTEM and corresponding high-resolution images of the Au/Si-NCs and Pt/Si-NCs. It is clear that, as compared with the as-prepared Si-NCs displayed in Fig. 1b, the morphology of the vertically aligned Si-NCs remains essentially intact after depositing the Au and Pt onto the Si-NC templates by rf-sputtering. The TEM image of the individual Au/Si-NC indicates that the Au film coated on Si-NC has a rather uneven droplet-like morphology (Fig. 3a). On the other hand, as displayed in Fig. 3c, the XTEM image for the Pt/Si-NC sample exhibits a very different morphology; the Pt layer appears to

Table 1 Field emission properties of bare Si-NCs and various thin films on Si-NCs. The turn-on field is defined at a current density of 10 μA cm^{-2}

Field emitter	Turn-on field (V μm^{-1})	Current density @ 5 V μm^{-1} (mA cm^{-2})	Work function (eV)	Reference
Au/Si-NCs	2.90	1.82	5.1	This study
Pt/Si-NCs	3.65	0.47	5.65	This study
Si-NCs	4.2	0.02	4.1	This study
Si-NWs	3.5	0.01 (@ 4.5 V μm^{-1})	4.1	6
SrTiO3/Si-tips	23	0.05 (@ 33 V μm^{-1})	3.69	18
$(Ba_{0.65}Sr_{0.3})_{1-x}La_xTiO_3$/Si	17	0.01 (@ 20 V μm^{-1})	3.2 (x = 0) 2.3 (x = 1)	19
ZnO/Si-NPs	0.74	0.20 (@ 1.7 V μm^{-1})	5.3	20
$CoSi_2$/TaN/Si-tips	7	0.015 (@ 13 V μm^{-1})	4.00 ($CoSi_2$/TaN) 4.39 (TaN)	23

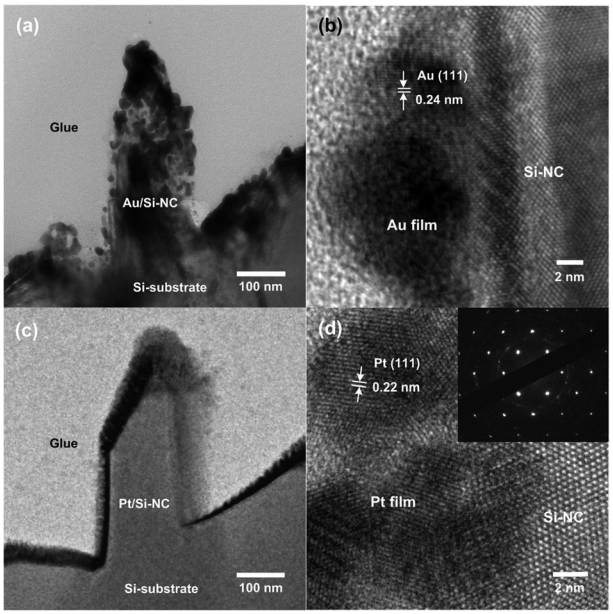

Fig. 3 The (a), (c) cross-sectional TEM and (b), (d) HRTEM image of the Au or Pt film on Si-NCs. The inset in (d) shows the diffraction pattern of Pt/Si-NCs.

cover the Si-NCs in a more uniform fashion, albeit an apparent shadowing effect is also evident. The HRTEM images shown in Fig. 3b and d give a closer look at the interface of Au/Si-NC and Pt/Si-NC heterostructures, respectively. It can be seen that the Pt layer deposited on the Si-NCs appears to form a continuous nano-crystalline film, as confirmed by the selected area diffraction (SAD) pattern (see the inset in Fig. 3d) and the distance between two adjacent planes (0.22 nm) indicated, which corresponds to the 111 planes of face-center-cubic (fcc) structured Pt.[24] In contrast, the morphology of the Au layer appears to comprise a relatively flat layer region of about 4 nm-thickness followed by discrete islands. The distance between the two adjacent planes in the island is ~0.24 nm (as indicated in Fig. 3b corresponding to the 111 planes of fcc-structured Au).[25] It has been pointed out by Landree *et al.*[26] that, for Au deposited on the Si(100) substrate at room-temperature, the growth mechanism follows the Stranski–Krastanov growth mode (layers plus islands) and there exists an amorphous glassy layer attributable to high entropy of mixing in the Au–Si system. Alternatively, Narusawa *et al.*[27] pointed out that the interface between Au film and the single crystal Si substrate tends to have a composition gradient within certain thickness (20–45 monolayers) to minimize the interfacial energy, even if the Au film is deposited at 20–50 °C. It is evident from Fig. 3b that the current result is more consistent with the scenario observed by Landree *et al.* On the other hand, due to the complexity of the Pt–Si phase diagram, platinum silicides can easily form at relatively low temperature and the presence of a thin SiO_x layer at the interface can even stabilize the morphology of the platinum silicide–silicon interface.[28] Unfortunately, most of the previous reports on the Pt/Si system were obtained with a certain degree of annealing at relatively elevated temperatures (*e.g.* 165–700 °C),[29] it is not clear whether or not the similar Pt-silicides could be formed at room-temperature and hence influence the morphology of the Pt films. Nevertheless, as indicated by the results displayed in Fig. 3d, the Pt layer deposited at room-temperature appears to follow the Volmer–Webber (island) growth mechanism and results in very different film morphology from that of the Au layer. Moreover, it is noted that in both cases there appears no SiO_x layer existing at the metal/Si-NC interfaces, which might ultimately affect the field emission properties of these heterostructures.

To further delineate the correlations between the obtained microstructure and the emission behavior, the *J–E* results are analyzed using the well-known Fowler–Nordheim (F–N) eqn (1):[30]

$$J = \frac{A\beta^2 E^2}{\varphi}\exp\left(-\frac{B\varphi^{3/2}}{\beta E}\right) \quad (1)$$

where J is the current density (A m^{-2}), E is the applied field (V μm^{-1}), φ is the work function (eV), β is the field enhancement factor, A and B are constants with $A = 1.56 \times 10^{-10}$ (A eV V^{-2}) and $B = 6.83 \times 10^3$ (V μm^{-1} $eV^{3/2}$), respectively. The inset (a) in Fig. 2a shows the plots of $\ln(J/E^2)$ *vs.* $1/E$ (the so called F–N plot) for the Au/Si-NCs (solid circles) and Pt/Si-NCs (solid triangles), respectively. It is clear that both sets of data can be fit by a straight line satisfactorily, indicating that the emission behavior follows the F–N model (eqn (1)) reasonably well. The slopes obtained for the Au/Si-NCs and Pt/Si-NCs are ~25 and ~40, respectively. From eqn (1), the field enhancement factor β can be related to the slope of the F–N plot with the following expression:[31,32]

$$\beta = -6.83 \times 10^3 \times \phi^{3/2}/\text{slope} \quad (2)$$

Thus, if we assume that β remains the same for Au/Si-NCs and Pt/Si-NCs owing to their similarities in emitter morphology, the difference in the slope of the F–N plots should be solely arising from the work functions. However, by taking $\phi_{Au} = 5.1$ eV and $\phi_{Pt} = 5.65$ eV from the literature,[33] it is obvious that the work function alone is inadequate to account for the observed difference in the slope of F–N plots. On the other hand, if we use the respective work function for Au and Pt and eqn (2), the obtained β values for Au/Si-NCs and Pt/Si-NCs are 2945 and 2395, respectively. The obtained β values for both metal-coated Si-NCs are in fact adequate for various applications of field emission. Furthermore, based on numerical computation,[34] the screening effect can be significant for dense nanostructures. The field enhancement for cylindrical emitters can also be estimated based on the geometric parameters by using:[20]

$$\beta \approx 1 + s\,(d/r) \quad (3)$$

where s is the field screening parameter, d is the distance between the emitter tip and the anode, and r is the radius of the emitter tips, respectively. By assuming $s \approx 1$, and taking d = 200 μm and $r \sim 30$ nm (as shown in Fig. 3a and c), the estimated β value is about 6700, suggesting that a substantial field screening effect with $s \approx 0.4$ is operating in this case. This also implies that there is ample room for improving the field

emission characteristics of the present structures provided the packing density can be reduced.

From the above observations, it is apparent that the enhancement of the field emission characteristics in metal-coated Si-NCs is a combination of various effects. In addition to the geometric effect and effective work function discussed above, we note that the resistivity of the coated metal may also play an important role. For instance, in the present study, the emission current densities at 5 V μm^{-1} are 0.47 and 1.82 A cm^{-2} for Pt/Si-NCs and Au/Si-NCs, respectively. The ratio is in fact very close to the resistivity ratio between Pt ($\rho \sim 11 \times 10^{-8}\ \Omega$ m) and Au ($\rho \sim 2.44 \times 10^{-8}\ \Omega$ m).[35] In any case, according to the data of field emission displayed in Table 1, the present study has evidently demonstrated the feasibility of incorporating a metal layer into Si-nanostructures using a relatively simple process scheme to obtain excellent field emission performance, which might have significant implications for future electron emission applications.

Conclusion

In summary, we have demonstrated a simple scheme for obtaining well-aligned Si-NCs, which comprises only a single-step Ag sputtering and a subsequent dry etching process. Further coating with Au and Pt layers onto such Si-NCs resulted in drastic improvement in field emission performances, namely the turn-on field could be reduced to 2.45 V μm^{-1} and current density of $\sim$1.82 mA cm^{-2} at 5 V μm^{-1} was achieved. The microstructural analyses indicated that Au and Pt exhibited very different growth behavior on Si-NC surfaces during the room-temperature sputtering deposition, albeit similar deposition parameters were practiced. The growth behavior was discussed in association with the intrinsic phase diagrams of both systems. The absence of interface oxide in both cases might explain the simple Fowler–Nordheim behavior exhibited in these metal–semiconductor heterostructure emitters. The field emission characteristics analyzed following the F–N model indicated a significant field screening effect still present, which might point a way for further improvements. Nevertheless, compared to those obtained from various surface-modified Si-nanostructures, such as ZnO/Si-nanopillars and ferroelectrics/Si-nanotips, the current results represent an interesting alternative route for producing surface-modified Si-NCs that might be useful for optical and electronic applications.

Acknowledgements

This work was partially supported by the National Science Council of Taiwan, under Grant No.: NSC 101-2811-M-009-044 and Center of Measuring Standards, ITRI, Taiwan, under contract: B301AA4231. J.-Y. Juang is supported in part by the National Science Council of Taiwan and the MOE-ATU program operated at NCTU. The authors would like to thank Dr. Wen-Shou Tseng and Dr. Yu-Hwa Shih for useful discussions. Prof. Hsi-Fu Shih (NCHU), Prof. Ching-Liang Dai (NCHU), and Jyun-Hao Wu (NCHU) are also gratefully acknowledged for helping with sputtering.

Notes and references

1 V. S. Kale, R. R. Prabhakar, S. S. Pramana, M. Rao, C.-H. Sow, K. B. Jinesh and S. G. Mhaisalkar, *Phys. Chem. Chem. Phys.*, 2012, **14**, 4614.
2 X. Wang and K. M. Liew, *J. Phys. Chem. C*, 2011, **115**, 10388.
3 L. He, C. Jiang, Rusli, D. Lai and H. Wang, *Appl. Phys. Lett.*, 2011, **99**, 021104.
4 S. Thiyagu, P. Devi, Z. Pei and Y.-C. Chen, Nanotechnology (IEEE-NANO), 10th IEEE Conference 2010, 320.
5 B. Wang, T. Stelzner, R. Dirawi, O. Assad, N. Shehada, S. Christiansen and H. Haick, *ACS Appl. Mater. Interfaces*, 2012, **4**, 4251.
6 Y.-F. Tzeng, H.-C. Wu, P.-S. Sheng, N.-H. Tai, H. T. Chiu, C. Y. Lee and I.-N. Lin, *ACS Appl. Mater. Interfaces*, 2010, **2**, 331.
7 H.-C. Wu, H.-Y. Tsai, H.-T. Chiu and C.-Y. Lee, *ACS Appl. Mater. Interfaces*, 2010, **2**, 3285.
8 J. P. Thomas, H.-C. Chen, S.-H. Tseng, H.-C. Wu, C.-Y. Lee, H. F. Cheng, N.-H. Tai and I.-N. Lin, *ACS Appl. Mater. Interfaces*, 2012, **4**, 5103.
9 Y. Yang, G. Meng, X. Liu, L. Zhang, Z. Hu, C. He and Y. Hu, *J. Phys. Chem. C*, 2008, **112**, 20126.
10 T.-H. Chang, K. Panda, B. K. Panigrahi, S.-C. Lou, C. Chen, H.-C. Chan, I.-N. Lin and N.-H. Tai, *J. Phys. Chem. C*, 2012, **116**, 19867.
11 J. Liu, V. V. Zhirnov, G. J. Wojak, A. F. Myers, W. B. Choi, J. J. Hren, S. D. Wolter, M. T. McClure, B. R. Stoner and J. T. Glass, *Appl. Phys. Lett.*, 1994, **65**, 2842.
12 Z. Pan, H.-L. Lai, F. C. K. Au, X. Duan, W. Zhou, W. Shi, N. Wang, C.-S. Lee, N.-B. Wong, S.-T. Lee and S. Xie, *Adv. Mater.*, 2000, **12**, 1186.
13 N. G. Shang, F. Y. Meng, F. C. K. Au, Q. Li, C. S. Lee, I. Bello and T. Lee, *Adv. Mater.*, 2002, **14**, 1308.
14 S.-C. Tseng, H.-L. Chen, C.-C. Yu, Y.-S. Lai and H.-W. Liu, *Energy Environ. Sci.*, 2011, **4**, 5020.
15 F.-W. Yuan, H.-J. Yang and H.-Y. Tuan, *J. Mater. Chem.*, 2011, **21**, 13793.
16 B. Zeng, G. Xiong, S. Chen, S. H. Jo, W. Z. Wang, D. Z. Wang and Z. F. Ren, *Appl. Phys. Lett.*, 2006, **88**, 213108.
17 B. Zeng, G. Xiong, S. Chen, W. Wang, D. Z. Wang and Z. F. Ren, *Appl. Phys. Lett.*, 2007, **90**, 033112.
18 H. J. Bian, X. F. Chen, J. S. Pan, W. Zhu and C. Q. Sun, *J. Appl. Phys.*, 2009, **105**, 013312.
19 H. Lu, J. S. Pan, X. F. Chen and W. G. Zhu, *J. Appl. Phys.*, 2007, **102**, 014113.
20 Y.-M. Chang, M.-C. Liu, P.-H. Kao, C.-M. Lin, H.-Y. Lee and J.-Y. Juang, *ACS Appl. Mater. Interfaces*, 2012, **4**, 1411.
21 A. Bondi, *Chem. Rev.*, 1953, **52**, 417.
22 Y.-M. Chang, J. Shieh and J.-Y. Juang, *J. Phys. Chem. C*, 2011, **115**, 8983.
23 B. W. Han, J. S. Lee and B. T. Ahn, *IEEE Electron Device Lett.*, 2002, **23**, 10.
24 N. C. Bigall, T. Hartling, M. Klose, P. Simon, L. M. Eng and A. Eychmuller, *Nano Lett.*, 2008, **8**, 4588.

25 D. Huang, X. Bai and L. Zheng, *J. Phys. Chem. C*, 2011, **115**, 14641.
26 E. Landree, D. Grozea, C. Collazo-Davila and L. D. Marks, *Phys. Rev. B: Condens. Matter Mater. Phys.*, 1997, **55**, 7910.
27 T. Narusawa, S. Komiya and A. Hiraki, *Appl. Phys. Lett.*, 1973, **22**, 389.
28 E. Conforto and P. E. Schmid, *Philos. Mag. A*, 2001, **81**, 61.
29 E. Conforto and P. E. Schmid, *Thin Solid Films*, 2008, **516**, 7467.
30 Y.-M. Chang, J.-M. Huang, C.-M. Lin, H.-Y. Lee, S.-Y. Chen and J.-Y. Juang, *J. Phys. Chem. C*, 2012, **116**, 8332.
31 Y.-M. Chang, P.-H. Kao, M.-C. Liu, C.-M. Lin, H.-Y. Lee and J.-Y. Juang, *RSC Adv.*, 2012, **2**, 11089.
32 Y.-M. Chang, M.-L. Lin, T.-Y. Lai, H.-Y. Lee, C.-M. Lin, Y.-C. S. Wu and J.-Y. Juang, *ACS Appl. Mater. Interfaces*, 2012, **4**, 6676.
33 H. B. Michaelson, *J. Appl. Phys.*, 1977, **48**, 4729.
34 V. Filip, D. Nicolaescu, M. Tanemura and F. Okuyama, *Ultramicroscopy*, 2001, **89**, 39.
35 R. A. Serway, J. W. Jewett Jr., S.-F. Tsai, J.-Y. Juang and T.-J. Yang, *Principles of physics a calculus approach*, Cengage Learning Asia Pte. Ltd., 2011, p. 756.

